

Excursion Set Halo Mass Function and Bias in a Stochastic Barrier Model of Ellipsoidal Collapse

P.S. Corasaniti and I. Achitouv
*Laboratoire Univers et Théories (LUTH), UMR 8102 CNRS,
Observatoire de Paris, Université Paris Diderot,
5 Place Jules Janssen, 92190 Meudon, France*

We use the Excursion Set formalism to compute the properties of the halo mass distribution for a stochastic barrier model which encapsulates the main features of the ellipsoidal collapse of dark matter halos. Non-markovian corrections due to the sharp filtering of the linear density field in real space are computed with the path-integral technique introduced by Maggiore & Riotto [20]. Here, we provide a detailed derivation of the results presented in [22] and extend the mass function analysis to higher redshift. We also derive an analytical expression for the linear halo bias. We find the analytically derived mass function to be in remarkable agreement with N-body simulation data from Tinker et al. [10] with differences $\lesssim 5\%$ over the range of mass probed by the simulations. The excursion set solution from Monte Carlo generated random walks shows the same level of agreement, thus confirming the validity of the path-integral approach for the barrier model considered here. Similarly the analysis of the linear halo bias shows deviations no greater than 20%. Overall these results indicate that the Excursion Set formalism in combination with a realistic modeling of the conditions of halo collapse can provide an accurate description of the halo mass distribution.

I. INTRODUCTION

Dark matter (DM) is an essential ingredient of the Standard Model of Cosmology. Observations provide strong evidence that about 90% of the matter in cosmic structures consists of such an invisible component [1–4]. Central to the DM paradigm is the idea that initial DM density fluctuations grow under gravitational instability fostering the collapse of baryonic matter. At late time, the gravitational infall becomes highly non-linear and DM particles violently relax into virialized objects, the halos. These are the building blocks in which cooling baryonic gas falls in to form the stars and galaxies that we observe today. Hence, the study of the halo mass distribution is of primary importance in Cosmology and an accurate modeling of the halo mass function has become essential to disclosing the complex mechanisms of the cosmic structure formation as well as probing the physics of the early universe. For example, recent studies have focused on the computation of the mass function for non-Gaussian initial conditions which are a direct signature of inflationary physics (see e.g. [5–7]).

The upcoming generation of galaxy cluster surveys (see e.g. [8, 9]) will directly probe the distribution of massive halos, thus providing cosmological constraints complementary to those inferred from measurements of the Cosmic Microwave Background (CMB) radiation and cosmic distance indicators.

The properties of the DM halo mass distribution have been mainly investigated using high-resolution numerical N-body simulations. These studies have determined the halo mass function to a few percent accuracy level and provided insights on its redshift and cosmology dependence [10–13]. In contrast, the development of purely theoretical studies has lagged behind. To date, a robust theoretical description of the halo mass function is still missing. For instance, we do not have a complete under-

standing of the relation between the conditions that lead to the formation of halos and the form of the mass function as obtained from N-body simulations. The numerical analysis usually limits to providing fitting formulae which depends on several ad-hoc parameters.

The seminal work by Press & Schechter (PS) [14] is the first to attempt a derivation of the halo mass function from the statistical properties of the initial dark matter density fluctuation field. The idea is that halos form in regions in which the linearly extrapolated density field, smoothed on a given scale, lies above a given critical threshold of collapse, such as that predicted from the spherical collapse model [15]. The PS formula explicitly depends on such a threshold, which introduces an exponential cut-off in the high-mass end as confirmed by N-body simulation analysis. However, the PS computation suffers of an inconsistent behavior when the variance becomes arbitrarily large. In this asymptotic regime it is natural to expect that the mass fraction tends to 1 (i.e. the higher the amplitude of the density fluctuations the larger is the fraction of mass in halos). However, in the PS case one finds 1/2, thus suggesting that half of the mass in halos has been somehow miscounted. This is the so called ‘cloud-in-cloud’ problem (see e.g. [16] and discussion therein).

The formulation of the Excursion Set theory by Bond et al. [17] has provided the Press-Schechter approach with a powerful mathematical formalism in which the computation of the mass function is reduced to solving a stochastic calculus problem (for an exhaustive review of the formalism see [18]). As shown in [17] the smoothed density fluctuation field behaves as a stochastic variable performing a random walk as function of the smoothing scale. Then, halos are associated to random trajectories which first cross a critical density threshold of collapse. It is the requirement of first-crossing which provides the solution to the ‘cloud-in-cloud’ problem. Nevertheless, the

computation of the halo mass function for realistic halo mass definitions has remained a challenging task. In fact, in the Excursion Set theory the mass of a halo depends on the form of the filter function, with the latter determining the behavior of the random walks. For realistic mass definitions the associated filters cause the random walks to be correlated, consequently the mass function can be estimated only through numerical Monte Carlo simulations [17, 19]. Because of this, a thorough systematic comparison of the Excursion Set mass function obtained accounting for such correlations against N-body simulation data has never been performed.

A major breakthrough in this direction has been recently made by Maggiore & Riotto [20] who have introduced path-integral techniques to perform an analytic computation of the halo mass function for generic filters. This allows us to consistently compare the Excursion Set model predictions with N-body data as well with astrophysical measurements of halo abundances.

Here, we compute the halo mass function and the linear halo bias for a barrier model which captures the main features of the ellipsoidal collapse of halos over a large range of masses. In this paper we also provide a detailed derivation of the results presented in [22].

The paper is organized as follows. In Section II we briefly introduce the Excursion Set formalism, in Section III we discuss the modeling of the non-spherical collapse of halos and the computation of the mass function. In Section IV we present the calculation of the corrections due to the filter function. In Section V we discuss the results of the comparison with N-body simulation data. In Section VI we present the computation of the halo bias. Finally, we present our conclusion in Section VII.

II. THE HALO MASS FUNCTION AND THE EXCURSION SET FORMALISM

In the Press-Schechter approach halos form from regions of the smoothed linear density fluctuation field which lie above a given density threshold. In such a case, the number of halos in the mass range $[M, M + dM]$ can be written as

$$\frac{dn}{dM} = f(\sigma) \frac{\bar{\rho}}{M^2} \frac{d \log \sigma^{-1}}{d \log M}, \quad (1)$$

where $\bar{\rho}$ is the background matter density and $\sigma(M)$ is the root-mean-square fluctuation of the linear dark matter density field smoothed on a scale $R(M)$ (containing a mass M) which is given by

$$\sigma^2(M) \equiv S(M) = \frac{1}{2\pi^2} \int dk k^2 P(k) \tilde{W}^2[k, R(M)], \quad (2)$$

where $P(k)$ is the linear matter power spectrum at redshift $z = 0$ and $\tilde{W}(k, R)$ is the Fourier transform of the smoothing (filter) function in real space. The function

$f(\sigma)$ in Eq. (1) is usually dubbed as ‘multiplicity function’ and encodes all the effects responsible for the formation of halos. It is given by $f(\sigma) = 2\sigma^2 \mathcal{F}(\sigma^2)$ where $\mathcal{F}(S) = dF/dS$ and $F(S)$ gives the fraction of mass elements in halos with mass $> M$. The goal of the Excursion Set computation is to evaluate $\mathcal{F}(S)$ and infer $f(\sigma)$. Hereafter, we will refer to $f(\sigma)$ simply as the mass function.

Let us briefly review the Excursion Set formalism. The density perturbation is defined as $\delta(\mathbf{x}) = [\rho(\mathbf{x}) - \bar{\rho}]/\bar{\rho}$, where $\rho(\mathbf{x})$ is the local density at the comoving position \mathbf{x} . Then, the smoothed density fluctuation field on a scale R is then given by

$$\delta(\mathbf{x}, R) = \int d^3y W(|\mathbf{x}-\mathbf{y}|, R) \delta(\mathbf{y}), \quad (3)$$

where $W(x, R)$ is the filter function in real space. In Fourier space, Eq. (3) reads as

$$\delta(\mathbf{x}, R) = \frac{1}{(2\pi)^3} \int d^3k \tilde{W}(k, R) \tilde{\delta}(\mathbf{k}) e^{-i\mathbf{k} \cdot \mathbf{x}} \quad (4)$$

where $\tilde{\delta}(\mathbf{k})$ is the Fourier transform of $\delta(\mathbf{x})$. Bond et al. [17] showed that by taking the derivative with respect to R , at any point in space $\delta(\mathbf{x}, R)$ obeys a Langevin equation of the form:

$$\frac{\partial \delta}{\partial R} = \zeta(R), \quad (5)$$

where

$$\zeta(R) \equiv \frac{1}{(2\pi)^3} \int d^3k \tilde{\delta}(\mathbf{k}) \frac{\partial \tilde{W}}{\partial R} e^{-i\mathbf{k} \cdot \mathbf{x}}, \quad (6)$$

is a noise term, whose properties depends on the statistics of the underlying density field. For initial Gaussian density fluctuations,

$$\langle \tilde{\delta}(\mathbf{k}) \rangle = 0 \text{ and } \langle \tilde{\delta}(\mathbf{k}) \tilde{\delta}(\mathbf{q}) \rangle = (2\pi)^3 \delta_D(\mathbf{k} + \mathbf{q}) P(k),$$

where δ_D is the Dirac-function, thus implying that $\langle \zeta(R) \rangle = 0$ and

$$\langle \zeta(R_1) \zeta(R_2) \rangle = \frac{1}{2\pi^2} \int dk k^2 P(k) \frac{\partial \tilde{W}}{\partial R_1} \frac{\partial \tilde{W}}{\partial R_2}. \quad (7)$$

Halos corresponds to those random walks which hit for the first time an absorbing barrier whose value is specified by a critical density threshold of collapse. In the spherical collapse model this is usually denoted by δ_c .

From Eq. (7) it is evident that the nature of the random walks depends on the form of the filter function. For the time being, let us assume the sharp-k filter,

$$\tilde{W}(k, R) = \theta(1/R - k), \quad (8)$$

then by substituting in Eq. (7) and after some algebraic manipulation we obtain

$$\frac{\partial \delta}{\partial S} = \eta_\delta(S), \quad (9)$$

with $\langle \eta_\delta(S) \rangle = 0$ and $\langle \eta_\delta(S_1)\eta_\delta(S_2) \rangle = \delta_D(S_1 - S_2)$. Hence, for the sharp-k filter $\eta(S)$ is a white noise and δ performs a simple Markov random walk as function of the variance S .

Let us define Π the probability of a trajectory to have value δ at time S . Then, the probability distribution associated to trajectories obeying Eq. (9), which start at $\delta(0) = 0^1$ and are absorbed by the spherical collapse barrier $B = \delta_c$, is given by the Fokker-Planck

$$\frac{\partial \Pi}{\partial S} = \frac{1}{2} \frac{\partial^2 \Pi}{\partial \delta^2}, \quad (10)$$

with initial condition $\Pi(\delta, S=0) = \delta_D(\delta)$ and absorbing boundary $\Pi(\delta_c, S) = 0$. This solution is

$$\Pi(\delta_c, \delta, S) = \frac{1}{\sqrt{2\pi S}} \left[e^{-\frac{\delta^2}{2S}} - e^{-\frac{(2\delta_c^2 - \delta)^2}{2S}} \right], \quad (11)$$

defined for $\delta < \delta_c$. Hence, the fraction of volume occupied by halos, i.e. the fraction of trajectories which have crossed the barrier ($\delta > \delta_c$) is given by $F(S) = 1 - \int_{-\infty}^{\delta_c} \Pi(\delta_c, \delta, S) d\delta$. Evaluating the first-crossing distribution dF/dS and substituting in the definition of $f(\sigma)$ we finally obtain

$$f(\sigma) = \frac{\delta_c}{\sigma} \sqrt{\frac{2}{\pi}} e^{-\frac{\delta_c^2}{2\sigma^2}}, \quad (12)$$

that is the ‘Extended Press-Schechter’ (EPS) mass function. In the next Sections we will discuss how a different choice of the halo collapse model and the smoothing function alter this standard result.

III. HALO COLLAPSE AND THE DIFFUSIVE DRIFTING BARRIER

The spherical collapse model [15] provides a complete description of the non-linear evolution of a spherically symmetric top-hat density perturbation embedded in a Friedman-Lemaitre-Robertson-Walker background. A characteristic feature of this model is that the collapse does not depend on the initial size of the region, i.e. on the initial radius, but only on the amplitude of the initial top-hat overdensity. Since the enclosed mass depends on the initial radius, then halos will be indistinctly associated to regions of the linear density field which lies above the same density threshold.

The work of Doroshkevich [23] has shown that initial Gaussian density perturbations are highly non-spherical and approximately triaxial. Hence, the collapse of a homogeneous ellipsoid (see e.g. [24]) should provide a far better description of the conditions of halo formation. In such a case the collapse depends on the initial overdensity

as well as the shear field and thus on the initial size of the ellipsoidal region, i.e. on the enclosed mass. Moreover, as also shown in [23], because of the random nature of the density perturbation field, the parameters characterizing the ellipsoid are random variables themselves with probability distributions which depend on the statistics of the underlying density fluctuation field. Consequently, the main feature of the non-spherical collapse of halos is that the critical density threshold is a stochastic variable itself. In the language of the Excursion Set this translates into a ‘fuzzy’ barrier performing a random walk whose properties depend on the specificity of the non-spherical collapse model considered (see e.g. [25–27]). For example, Sheth et al. [28] have shown that in the ellipsoidal collapse model the barrier on average evolves as $\langle B \rangle = \delta_c [1 + \beta(S/\delta_c^2)^\gamma]$, with $\beta = 0.47$ and $\gamma = 0.615$. This trend reflects the fact that in the small mass range (large S) there is a significant shear that opposes the gravitational infall, hence a higher density threshold is needed for the collapse to occur. Instead, for large masses the shear field is less significant, halos are more isolated and the collapse is approximately spherical.

Moving barrier models have been considered in a variety of case studies. Sheth [29] has introduced a linear barrier model to study the halo distribution in Eulerian space. In [30] barriers with different functional dependence on S were used to model the formation of halos, filaments and sheets, while in [31] a moving barrier has been introduced to infer the size distribution of H II bubbles during reionization. These studies have used Monte-Carlo simulations to infer the mass distribution. Alternatively, Zhang & Hui [32] have introduced an integral-equation method which allows for a recursive computation of the mass function for generic moving barriers without requiring the use of Monte-Carlo simulations. Nevertheless, all these studies have focused on rigid moving barriers rather than stochastic ones. A realistic description of the non-spherical collapse conditions of DM halos must necessarily account for this characteristic feature that, as we will see here, modifies the EPS result in a very distinctive way. Furthermore, the analysis of numerical N-body simulations has indeed confirmed the stochastic barrier hypothesis. For instance, the work by Robertson et al. [33] has clearly shown that the linear density fluctuation associated with halos detected in the numerical simulations at a given redshift has not a unique constant value, but is randomly distributed as function of the halo mass, following an approximately log-normal distribution with a nearly linearly drifting average.

Maggiore & Riotto [21] have implemented these features in the Excursion Set theory by assuming a Gaussian diffusive barrier with $\langle B \rangle = \delta_c$ and $\langle (B - \langle B \rangle)^2 \rangle = S D_B$, where D_B is a constant diffusion coefficient which they set to $D_B \approx 0.3$ to reproduce the results of [33]. Here, we improve the modeling of the diffusive stochastic barrier by assuming a linearly drifting average, $\langle B \rangle \equiv \bar{B}(S) = \delta_c + \beta S$ (see e.g. [29]), which approximates the average drift predicted by the ellipsoidal collapse model in [28].

¹ At very large scales $S \rightarrow 0$ and density perturbation $\delta \rightarrow 0$.

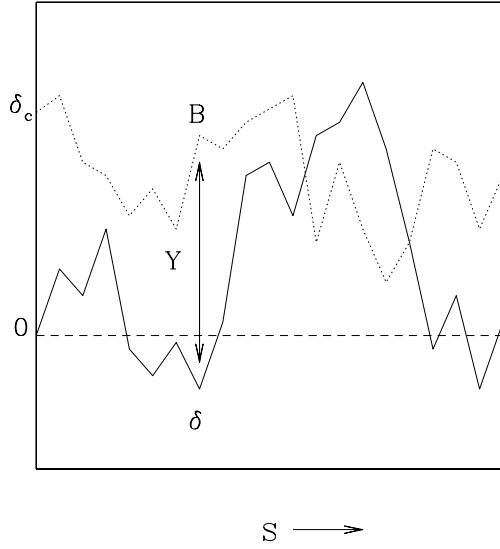


FIG. 1: Schematic representation of random walk trajectories for δ (solid line) and the barrier B (dot line) as function of the variance. The variable $Y = B - \delta$ measure the distance between the two trajectories and therefore performs a random walk as well. The trajectories starts at $\delta(0) = 0$ and $B(0) = \delta_c$, i.e. $Y(0) = \delta_c$.

Under these assumptions the barrier obeys the following Langevin equation

$$\frac{\partial B}{\partial S} = \beta + \eta_B(S), \quad (13)$$

where the noise $\eta_B(S)$ is characterized by $\langle \eta_B(S) \rangle = 0$ and $\langle \eta_B(S)\eta_B(S') \rangle = D_B \delta_D(S - S')$. Without loss of generality we can assume that $\eta_B(S)$ and $\eta_\delta(S)$ are uncorrelated and the stochastic evolution of the system is described by Eqs. (9)-(13) with absorbing boundary at $\delta(S) = B(S)$. The system can be reduced to a one-dimensional random walk by introducing the variable $Y = B - \delta$. In such a case we have

$$\frac{\partial Y}{\partial S} = \beta + \eta(S), \quad (14)$$

with white noise $\eta(S) = \eta_\delta(S) + \eta_B(S)$ such that $\langle \eta(S) \rangle = 0$ and $\langle \eta(S)\eta(S') \rangle = (1 + D_B)\delta(S - S')$.

In Fig. 1 we plot a schematic representation of the random walks. The variable Y measures the distance of the trajectory of the density field to the barrier as function of the variance. The system starts at $S = 0$ with $\delta(0) = 0$ and $B(0) = \delta_c$, thus $Y(0) \equiv Y_0 = \delta_c$. Random walks which have yet to form halos correspond to $Y > 0$. The absorbing boundary is located at $Y = 0$ and trajectories which have collapsed into halos correspond to $Y < 0$. From Eq. (14) we derive the Fokker-Planck equation for the probability distribution $\Pi_0(Y_0, Y, S)$ of

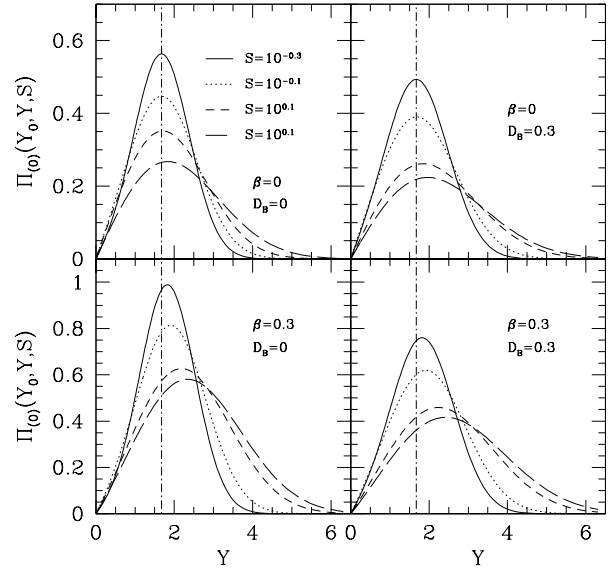


FIG. 2: Probability distribution of non-collapsing trajectories ($Y > 0$) for $S = 10^{-0.3}$ (solid line), $10^{-0.1}$ (dot line), $10^{0.1}$ (short dash line) and $10^{0.3}$ (long dash line). Top left panel: Extended Press-Schechter ($\beta = 0$, $D_B = 0$); top right panel: diffusive barrier ($\beta = 0$, $D_B = 0.3$); bottom left panel: linearly drifting barrier ($\beta = 0.3$, $D_B = 0$); bottom right panel: diffusive barrier with linearly drifting average ($\beta = 0.3$, $D_B = 0.3$).

the random walks with $Y > 0$ (see e.g. [34]):

$$\frac{\partial \Pi_0}{\partial S} = -\beta \frac{\partial \Pi_0}{\partial Y} + \frac{1 + D_B}{2} \frac{\partial^2 \Pi_0}{\partial Y^2}, \quad (15)$$

where the subscript ‘0’ refers to the fact that the random walks which we are considering are Markovian. We solve Eq. (15) with initial condition $Y_0 = \delta_c$ and impose the absorbing boundary condition at $Y = 0$, i.e. $\Pi_0(0, S) = 0$. By rescaling the variable $Y \rightarrow \tilde{Y} = Y/\sqrt{1 + D_B}$, a factorisable solution can be found in the form $\Pi_0(\tilde{Y}, S) = U(\tilde{Y}, S) \exp[c(\tilde{Y} - cS/2)]$, where $c = \beta/\sqrt{1 + D_B}$ and $U(\tilde{Y}, S)$ satisfies a Gaussian diffusion equation which can be solved using the image method [35] or by Fourier transform. We find

$$\Pi_0(Y_0, Y, S) = \frac{e^{-\frac{\beta}{1+D_B}(Y-Y_0-\beta\frac{S}{2})}}{\sqrt{2\pi S(1+D_B)}} \left[e^{-\frac{(Y-Y_0)^2}{2S(1+D_B)}} - e^{-\frac{(Y+Y_0)^2}{2S(1+D_B)}} \right]. \quad (16)$$

Here, it is worth remarking that a general analytic solution to the Fokker-Planck equation with biased diffusion and absorbing boundary condition does not exist for drift terms which are non-linear in S . As it will be evident in the next Section, having an analytical expression for the probability distribution of the Markovian random walk greatly simplifies the computation of the non-Markovian corrections induced by a realistic filtering of

the linear density field. For this very reason we have opted to assume a barrier model with linearly drifting average, rather than the ellipsoidal collapse prediction from [28].

In Fig. 2 we plot $\Pi_0(Y_0, Y, S)$ as function of Y at $S = 10^{-0.3}$ (solid line), $10^{-0.1}$ (dot line), $10^{0.1}$ (short dash line) and $10^{0.3}$ (long dash line) for different value of β and D_B such as to give us a qualitative understanding of the barrier model parameter dependence. The standard EPS result corresponds to $\beta = 0$ and $D_B = 0$ (top left panel). The case of a diffusive barrier with $\beta = 0$ and $D_B = 0.3$ (as in [21]) is shown in the top right panel, while the case of the linearly drifting average barrier with $\beta = 0.3$ and $D_B = 0$ is shown in the bottom left². Finally, the case of the diffusive barrier with linearly drifting average with $\beta = 0.3$ and $D_B = 0.3$ is plotted in the bottom right panel.

We may notice that overall amplitude of $\Pi_0(Y_0, Y, S)$ is a decreasing function of S with an increasing skewness toward larger values of Y . Since the total number of trajectories is conserved, this implies that the probability of trajectories that do not cross the barrier between Y and $Y + dY$ decreases as function of S , while that of those which first-cross it increases. This is consistent with that fact that in the bottom-up scenario small mass halos are more likely to form than large ones. However, at a finer level the trend is barrier model dependent. For instance in the case of the diffusive barrier (top right panel) we can see that the amplitude of $\Pi_0(Y_0, Y, S)$ is smaller than the standard EPS result (top left panel). Thus, indicating that the number of crossing trajectories is higher. In contrast, for the non-diffusive barrier with drifting average (bottom left panel) we have that $\Pi_0(Y_0, Y, S)$ is larger than the EPS prediction. In addition, the peak of the probability distribution rapidly shifts towards larger values of Y as function of S as opposed to the EPS case. Finally, for the diffusive barrier with linearly drifting average (bottom right panel) we may notice that the combined effect of diffusion and drift is to reduce the overall amplitude of $\Pi_0(Y_0, Y, S)$ more effectively in the large mass range than in the low mass end.

The first-crossing distribution gives by definition the probability $\mathcal{F}_0(S)$ of a random walk to cross the barrier between S and $S + dS$, thus we have:

$$\begin{aligned} \mathcal{F}_0(S) &= -\frac{\partial}{\partial S} \int_0^\infty dY \Pi_0(Y_0, Y, S) \\ &= \beta \Pi_0(Y_0, Y, S) \Big|_0^\infty - \frac{1 + D_B}{2} \frac{\partial \Pi_0}{\partial Y} \Big|_0^\infty \\ &= \frac{\delta_c}{S^{3/2} \sqrt{2\pi(1 + D_B)}} e^{-\frac{(\delta_c + \beta S)^2}{2S^2(1 + D_B)}}, \end{aligned} \quad (17)$$

² We find that for $\beta = 0.3$ the linear drifting average barrier $\bar{B}(S) = \delta_c + \beta S$ approximates to better than 10% the prediction of the ellipsoidal collapse model [28] over the range $-0.6 < \log(1/\sigma) < 0.4$.

for $D_B = 0$ this coincides with the non-diffusing linear drifting barrier solution found in [18]. Then, the Markovian mass function reads as:

$$f_0(\sigma) = \frac{\delta_c}{\sigma \sqrt{1 + D_B}} \sqrt{\frac{2}{\pi}} e^{-\frac{(\delta_c + \beta \sigma^2)^2}{2\sigma^2(1 + D_B)}}. \quad (18)$$

The competing effect of diffusion and average drift, which we have inferred from the qualitative analysis of $\Pi_0(Y_0, Y, S)$, can be seen directly in the form of Eq. (18). The non-vanishing diffusion coefficient has the effect of reducing the amplitude of the mass function cut-off, thus shifting it toward smaller values of σ . In contrast, the drift of the barrier tends to increase the value of the threshold as function of σ .

In Fig. 3 we plot $f_0(\sigma)$ for the same values of β and D_B shown in Fig. 2. The qualitative trend confirms that inferred from the analysis of $\Pi_0(Y_0, Y, S)$. Firstly, we notice that with respect to the standard EPS case (solid line), the diffusing barrier model (dot line) shows a cut-off at a lower value of σ . This is because in the presence of diffusion the condition of collapse has a scatter around the spherical collapse threshold which favors the trajectory crossing. Consequently, the mass function is larger than the EPS result over a larger range of masses. In contrast, the linear drifting barrier (short dash line) gives a mass function which is suppressed at all masses. This is consistent with the fact that the barrier is on average higher than the spherical collapse threshold, thus is more difficult for trajectories to cross the barrier. In the case of a diffusive barrier with linearly drifting average (long dash line) the combination of the two effects causes the mass function to be tilted with respect to the EPS prediction. In the next Section we will discuss the modifications to Eq. (18) due to a different choice of the smoothing function.

IV. NON-MARKOVIAN CORRECTIONS AND PATH-INTEGRAL APPROACH

A. Halo Mass Definition and Filter Function

The filtering of the linear density fluctuation field specifies the relation between the smoothing scale R and the mass M . The volume selected by the window function $W(x, R)$ is $V(R) = \int d^3x W(x, R)$, hence the enclosed mass is given by $M(R) = \bar{\rho}V(R)$. However, this relation is uniquely specified only for a sharp-x filter, $W(r, R) = \theta(r - R)$, for which $M(R) = 4/3\pi\bar{\rho}R^3$. For generic filters, the mass definition is ambiguous, since it is defined up to a normalization constant. More importantly, in the case of the sharp-k filter, $W(k, R) = \theta(1/R - k)$, the mass remains undefined (see discussion in [20]). On top of this, we should consider the fact that the mass definition of N-body halos depends on the halo detection algorithm. Thus, for a consistent model comparison with numerical simulations, the filtering of the linear density

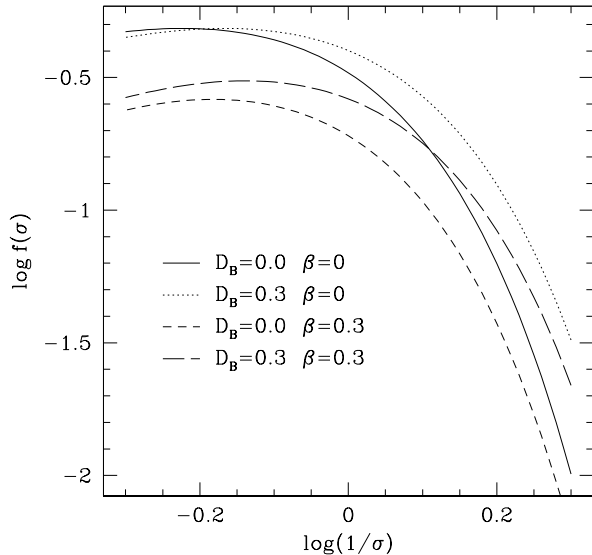


FIG. 3: Mass function for values of β and D_B as in Fig. 2.

field should be chosen consistently with the mass definition of the halo detection algorithm used to measure the N-body mass function. As an example, the Spherical Overdensity (SOD) halo finder detects halos as spherical regions of radius R_Δ enclosing a density $\rho_\Delta = \Delta \bar{\rho}$, where Δ is the overdensity parameter usually fixed to $\Delta = 200$ (which is roughly equal to spherical collapse prediction of the virial overdensity at $z = 0$ in LCDM models). In such a case, the halo mass is $M_\Delta = 4/3\pi\bar{\rho}\Delta R_\Delta^3$, that is equivalent to definition of the sharp-x filter. However, random walks generated by this smoothing function are no longer Markovian. In fact, the Fourier transform of the sharp-x filter is

$$\tilde{W}(k, R) = \frac{3}{(kR)^3} [\sin(kR) - (kR) \cos(kR)]. \quad (19)$$

and in such a case it is easy to see from Eq (7) that $\delta(S)$ is no longer subject to a simple white noise.

Maggiore & Riotto [20] have shown that the correlations induced by the filter function can be treated as perturbations about the Markovian solution. Let us consider a Gaussian random walk, the statistical properties are entirely specified by the 1 and 2-point connected correlators. For a Gaussian field these are $\langle \delta(R) \rangle_c = 0$ and

$$\langle \delta(R)\delta(R') \rangle_c = \int_0^\infty \frac{k^2 dk}{2\pi^2} P(k) \tilde{W}(k, R) \tilde{W}(k, R') \quad (20)$$

respectively, with $P(k) = A k^{n_s} T^2(k)$ and $T(k)$ is the matter transfer function. In the case of a sharp-k filter Eq. (20) simply reduces to $\langle \delta(R[S])\delta(R[S']) \rangle_c = \min(S, S')$. However, Maggiore & Riotto [20] have shown that for the sharp-x filter the 2-point connect correlator can be written as $\langle \delta(R[S])\delta(R[S']) \rangle_c = \min(S, S') +$

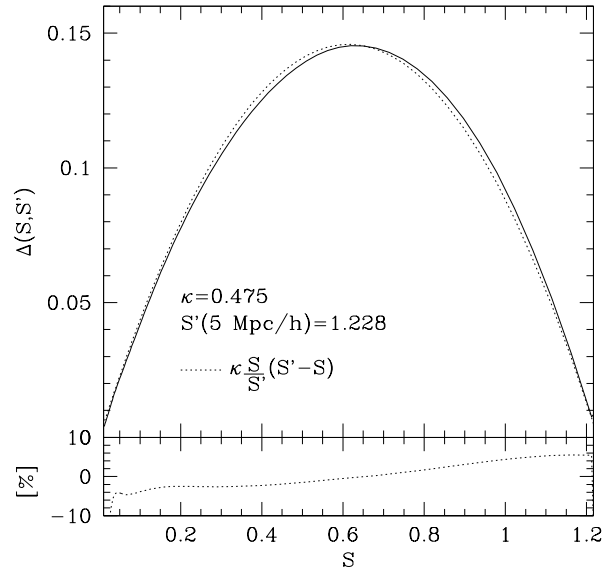


FIG. 4: Correlation function $\Delta(S, S')$ for a sharp-x filter (solid line) obtained by numerically integrating Eq. (20) for $S'(R=5 \text{ Mpc/h}) = 1.228$ in the range $0 < S < S'$, and the fitting function $\kappa S/S'(S' - S)$ with $\kappa = 0.475$ (dash line).

$\Delta(S, S')$, where $\Delta(S, S')$ is a symmetric function which vanishes at $S = S'$ and is well approximated by $\Delta(S, S') \approx \kappa S/S'(S' - S)$ and κ is a fitting coefficient. Following their computation, we estimate $\Delta(S, S')$ in a Λ CDM cosmology with model parameters set to the WMAP-5yr best fit values: $\Omega_M = 1 - \Omega_\Lambda = 0.28$, $h = 0.7$, $\sigma_8 = 0.8$ and $n_s = 0.96$. We compute the transfer function using the CMBFAST code [36]. In Fig. (4) we plot $\Delta(S, S')$ for $S'(R=5 \text{ Mpc/h}) = 1.228$ (solid line) against $\kappa S/S'(S' - S)$ for the best fit value $\kappa = 0.475$. We can see that difference between the numerically evaluated correlation function and the best fitting formula is well within a few per-cent level. Note that $\kappa = 0.475$ slightly differs from the value found in [20]. The discrepancy is due to the difference between the numerically computed CMBFAST transfer function and the approximate fitting formula by Sugiyama [37] which has been used in [20]. The coefficient κ depends on the assumed cosmological model and does not evolve in redshift. As pointed out in [20], a weakly linear dependence of κ on the smoothing scale R can improve the fit to the numerically computed correlation function $\Delta(S, S')$. Nevertheless, such dependence can be neglected to first approximation.

In terms of the variable Y the non-vanishing connected correlators read as $\langle Y(S) \rangle_c \equiv \bar{B}(S) = \delta_c + \beta S$ and $\langle Y(S)Y(S') \rangle_c = (1 + D_B)\min(S, S') + \Delta(S, S')$ respectively. Having assumed the barrier to perform Gaussian random walks implies that the non-Markovian part of the 2-point correlator identically vanishes, i.e. $\Delta_B(S, S') = 0$. One may wonder whether a term like $\Delta_B(S, S')$ due

to the filter function should also be included. However, there is no reason as to why the barrier has to have the same filtering of the linear density field, since the two smoothing procedures have very different physical meanings. The latter is related to the halo mass definition, while the former specifies the correlation between the condition of halo collapse at different scales. The simplest approximation is to assume that the collapse at a scale S is independent of that at S' , which is equivalent to having $\Delta_B(S, S') = 0$, i.e. Gaussian random walks. This suggests that a variety of non-linear gravitational effects which induce scale-dependent correlations of the halo collapse condition can be implemented in such a formalism through the barrier p -point connected correlators with $p \geq 2$ or using a non-trivial smoothing procedure of the barrier random walks.

B. Path-Integral Method

Hereafter, we will follow the derivation of [20], and extend the computation of the non-Markovian corrections the case of the diffusive barrier model with linearly drifting average.

Let us consider the random walk of the variable Y over the time interval $[0, S]$ discretized in steps $\Delta S = \epsilon$, such that $S_k = k\epsilon$ with $k = 1, \dots, n$. The probability

distribution of trajectories that start at Y_0 , end in Y_n at time S_n and which never cross the barrier is given by

$$\Pi_\epsilon(Y_0, Y_n, S_n) = \int_0^\infty dY_1 \dots \int_0^\infty dY_{n-1} W(Y_0, \dots, Y_n, S_n), \quad (21)$$

where

$$W(Y_0, \dots, Y_n, S_n) \equiv \langle \delta_D(Y(S_1) - Y_1) \dots \delta_D(Y(S_n) - Y_n) \rangle, \quad (22)$$

is the probability density distribution. Using the Fourier transform of the Dirac-function we have

$$W(Y_0, \dots, Y_n, S_n) = \int \mathcal{D}\lambda e^{i \sum_{i=1}^n \lambda_i Y_i} \langle e^{-i \sum_{i=1}^n \lambda_i Y(S_i)} \rangle, \quad (23)$$

with $\int \mathcal{D}\lambda = \int_{-\infty}^\infty \frac{d\lambda_1}{2\pi} \dots \frac{d\lambda_n}{2\pi}$. The exponential factor within the brackets can be written in terms of the connected correlators $\langle Y(S) \rangle_c$ and $\langle Y(S)Y(S') \rangle_c$

$$\langle e^{-i \sum_{i=1}^n \lambda_i Y(S_i)} \rangle = e^{-i \sum_{i=1}^n \lambda_i \bar{B}_i - \frac{1}{2} \sum_{ij} \lambda_i \lambda_j (A_{ij} + \Delta_{ij})} \quad (24)$$

where we have indicated with $\bar{B}_i = \bar{B}(S_i)$, $A_{ij} = (1 + D_B) \min(i, j)\epsilon$ and $\Delta_{ij} = \kappa S_i / S_j (S_j - S_i)$. Substituting Eq. (24) in Eq. (21) and given the fact that $\Delta_{ij} < 1$ we can expand in κ , to first order we have

$$\Pi_\epsilon(Y_0, Y_n, S_n) = \int_0^\infty dY_1 \dots \int_0^\infty dY_n \int \mathcal{D}\lambda \left(1 - \frac{1}{2} \sum_{ij} \lambda_i \lambda_j \Delta_{ij} \right) e^{-i \sum_k \lambda_k [\bar{B}_k - Y_k]} e^{-\frac{\kappa}{2} \sum_{ij} \lambda_i \lambda_j \tilde{A}_{ij}}, \quad (25)$$

where $\tilde{A}_{ij} = (1 + D_B) \min(i, j)$. Thus

$$\Pi_\epsilon(Y_0, Y_n, S_n) = \Pi_0^\epsilon(Y_0, Y_n, S_n) + \Pi_1^\epsilon(Y_0, Y_n, S_n), \quad (26)$$

where $\Pi_0^\epsilon(Y_0, Y_n, S_n)$ is the Markovian zero order term and $\Pi_1^\epsilon(Y_0, Y_n, S_n)$ is the first order correction in κ . The Markovian term obeys the Chapman-Kolmogorov equation (see Eq. (A6) in Appendix A for a detailed derivation) which is used to explicitly compute the non-Markovian term.

A crucial point concerns the ϵ -dependence of $\Pi_0^\epsilon(Y_0, Y_n, S_n)$ in the proximity of the barrier. As extensively discussed in [20], the Markovian solution $\Pi_0^\epsilon(Y_0, Y_n, S_n)$ is $\mathcal{O}(\epsilon)$ for $Y_n > 0$ and $\mathcal{O}(\epsilon^{1/2})$ at $Y_n = 0$. Hence the probability distribution undergoes a transition between two different regimes inside a boundary layer of finite size. In order to evaluate the form of the probability distribution inside this region it is convenient to introduce the ‘stretch’ variable $\eta = Y / \sqrt{2\epsilon(1 + D_B)}$ and write

$$\Pi_0^\epsilon(Y_0, Y_n, S_n) = C_\epsilon(Y_0, Y_n, S_n) u(\eta), \quad (27)$$

where $C_\epsilon(Y_0, Y_n, S_n)$ is a smooth solution and $u(\eta)$ is a

function containing the fast variation in ϵ inside the transition region. In the continuous limit, $\lim_{\eta \rightarrow \infty} u(\eta) = 1$, while C_ϵ tends to Eq. (16), thus we recover the standard Markovian solution. Substituting $Y \equiv Y_n = \eta \sqrt{2\epsilon(1 + D_B)}$ in Eq. (16) and expanding to lowest order in ϵ we obtain

$$C_\epsilon(Y_0, Y_n, S_n) = \sqrt{\epsilon} \frac{2\eta Y_0}{\sqrt{\pi} S_n^{3/2} (1 + D_B)} e^{-\frac{(Y_0 + \beta S_n)^2}{2S_n(1 + D_B)}}. \quad (28)$$

Hence, substituting Eq. (28) in Eq. (27) and taking the limit $\eta \rightarrow 0$ we obtain

$$\Pi_0^\epsilon(Y_0, 0, S_n) = \sqrt{\epsilon} \frac{\gamma Y_0}{S_n^{3/2} (1 + D_B)} e^{-\frac{(Y_0 + \beta S_n)^2}{2S_n(1 + D_B)}}, \quad (29)$$

where

$$\gamma \equiv \frac{2}{\sqrt{\pi}} \lim_{\eta \rightarrow 0} \eta u(\eta) = \frac{1}{\sqrt{\pi}}, \quad (30)$$

we present the exact derivation of this result in Appendix B.

Similarly we can infer the probability $\Pi_0^\epsilon(0, Y_n, S_n)$ of trajectories starting at the barrier $Y_0 = 0$ and ending at $Y_n > 0$ by introducing the stretch variable $\eta = Y_0/\sqrt{2\epsilon(1+D_B)}$. Again, substituting $Y_0 = \eta\sqrt{2\epsilon(1+D_B)}$ in Eq. (16), expanding to lowest order in ϵ and computing Eq. (27) in the limit $\eta \rightarrow 0$ we obtain

$$\Pi_0^\epsilon(0, Y_n, S_n) = \sqrt{\epsilon} \frac{\gamma Y_n}{S_n^{3/2}(1+D_B)} e^{-\frac{(Y_n - \beta S_n)^2}{2S_n(1+D_B)}}. \quad (31)$$

Finally, the probability of trajectories which start at the barrier and end at the barrier can be obtained using the dimensional arguments discussed in [20]. To lowest order in ϵ , we find

$$\Pi_0^\epsilon(0, 0, S_n) = \epsilon \frac{1}{S_n^{3/2} \sqrt{2\pi(1+D_B)}}. \quad (32)$$

C. Non-Markovian Corrections to the Halo Mass Function

We have now all the ingredients to compute the non-Markovian correction to first order in κ . Using the fact that $\lambda_i e^{-i\lambda_i[B_i - Y_i]} = -i\partial/\partial Y_i e^{-i\sum_{ij} \lambda_{ij} [B_k - Y_k]}$, the second term in Eq. (25) reads as

$$\begin{aligned} \Pi_1^\epsilon(Y_0, Y_n, S_n) &= \frac{1}{2} \sum_{ij} \int_0^\infty dY_1 \dots \int_0^\infty dY_{n-1} \Delta_{ij} \times \\ &\times \partial_i \partial_j W_0(Y_0, \dots, Y_n, S_n), \end{aligned} \quad (33)$$

where $W_0(Y_0, \dots, Y_n, S_n)$ is the Markovian probability density of the random walks (see Appendix A). We split the sum in Eq. (33) as

$$\frac{1}{2} \sum_{ij} \Delta_{ij} \partial_i \partial_j = \frac{1}{2} \Delta_{nn} \partial_n^2 + \sum_{i=1}^{n-1} \Delta_{in} \partial_i \partial_n + \sum_{i < j} \Delta_{ij} \partial_i \partial_j, \quad (34)$$

notice that the first term on the right-hand side of Eq. (34) vanishes since $\Delta_{nn} = 0$, furthermore $\sum_{i < j} = \sum_{i=1}^{n-2} \sum_{j=i+1}^{n-1}$. Then, integrating Eq. (33) by parts and using Eq. (A6) we obtain

$$\Pi_1^\epsilon(Y_0, Y_n, S_n) = \Pi_{\epsilon,1}^m(Y_0, Y_n, S_n) + \Pi_{\epsilon,1}^{m-m}(Y_0, Y_n, S_n), \quad (35)$$

where

$$\begin{aligned} \Pi_{\epsilon,1}^m(Y_0, Y_n, S_n) &= - \sum_{i=1}^{n-1} \Delta_{in} \partial_n \left[\Pi_0^\epsilon(Y_0, 0, S_i) \times \right. \\ &\times \left. \Pi_0^\epsilon(0, Y_n, S_n - S_i) \right], \end{aligned} \quad (36)$$

is a ‘memory’-like term, since it depends on a single sum over the past time steps, and

$$\begin{aligned} \Pi_{\epsilon,1}^{m-m}(Y_0, Y_n, S_n) &= \sum_{i=1}^{n-2} \sum_{j=i+1}^{n-1} \Delta_{ij} \left[\Pi_0^\epsilon(Y_0, 0, S_i) \times \right. \\ &\times \left. \Pi_0^\epsilon(0, 0, S_j - S_i) \Pi_0^\epsilon(0, Y_n, S_n - S_j) \right], \end{aligned} \quad (37)$$

which represents a ‘memory-of-memory’ term. For a detailed derivation of these equations see Appendix C. The probability distributions in Eq. (36) and (37) are given by Eq. (29), (31) and (32) respectively. In order to compute the sum over the time steps we take the continuous limit such that

$$\sum_{i=1}^{n-1} \rightarrow \frac{1}{\epsilon} \int_0^S dS_i \text{ and } \sum_{i < j} \rightarrow \frac{1}{\epsilon^2} \int_0^S dS_i \int_{S_i}^S dS_j.$$

We find that the ‘memory’ term not to contribute to the mass function. As a result of the integration over dS_i we have

$$\begin{aligned} \Pi_1^m(Y_0, Y, S) &= - \frac{\kappa Y_0}{(1+D_B)^2} \times \\ &\times \frac{\partial}{\partial Y} \left\{ Y e^{\frac{\beta}{1+D_B}(Y - Y_0 - \beta \frac{S}{2})} \text{Erfc} \left[\frac{Y_0 + Y}{\sqrt{2S(1+D_B)}} \right] \right\}, \end{aligned} \quad (38)$$

and since the first-crossing distribution is given by $\mathcal{F}_1^m = -\frac{\partial}{\partial S} \int_0^\infty dY \Pi_1^m(Y_0, Y, S)$, the subsequent integration of Eq. (38) over dY vanishes. This is consistent with the result of Maggione & Riotto [20].

The ‘memory-of-memory’ term cannot be computed analytically. Nevertheless, from the ellipsoidal collapse model we have $\beta < 1$. Thus, we can expand the integrands in powers of β and compute the contribution to the mass function up to leading order. We find

$$f_{1,\beta=0}^{m-m}(\sigma) = -\tilde{\kappa} \frac{\delta_c}{\sigma} \sqrt{\frac{2a}{\pi}} \left[e^{-\frac{a\delta_c^2}{2\sigma^2}} - \frac{1}{2} \Gamma \left(0, \frac{a\delta_c^2}{2\sigma^2} \right) \right], \quad (39)$$

where $a = 1/(1+D_B)$, $\tilde{\kappa} = \kappa a$ and $\Gamma(0, z)$ is the incomplete Gamma function. Not surprisingly this expression coincides with the κ -correction for the diffusive barrier obtained in [21]. The first order in β reads as

$$f_{1,\beta^{(1)}}^{m-m}(\sigma) = -\beta a \delta_c \left[f_{1,\beta=0}^{m-m}(\sigma) + \tilde{\kappa} \text{Erfc} \left(\frac{\delta_c}{\sigma} \sqrt{\frac{a}{2}} \right) \right], \quad (40)$$

while the second order is given by

$$\begin{aligned} f_{1,\beta^{(2)}}^{m-m}(\sigma) &= \beta^2 a \delta_c \tilde{\kappa} \left\{ a \delta_c \text{Erfc} \left(\frac{\delta_c}{\sigma} \sqrt{\frac{a}{2}} \right) + \right. \\ &+ \left. \sigma \sqrt{\frac{a}{2\pi}} \left[e^{-\frac{a\delta_c^2}{2\sigma^2}} \left(\frac{1}{2} - \frac{a\delta_c^2}{\sigma^2} \right) + \frac{3}{4} \frac{a\delta_c^2}{\sigma^2} \Gamma \left(0, \frac{a\delta_c^2}{2\sigma^2} \right) \right] \right\}. \end{aligned} \quad (41)$$

Higher order corrections can be computed semi-analytically, since these contain integrals that cannot be written in terms of basic functions. Simple numerical integration routines are sufficient to evaluate these integrals. Nevertheless, we find that for $\beta/(1+D_B) < 1$ terms $\mathcal{O}(> \beta^2)$ are negligible. For example in Fig. 5 we plot the Markovian mass function f_0 and the κ -corrections up to $\mathcal{O}(\beta^3)$ and their total contribution for $\beta = 0.2$ and $D_B = 0.6$. We can see that the term $\mathcal{O}(\beta^3)$ is negligible. The largest non-Markovian corrections are

given by $f_{1,\beta=0}^{m-m}(\sigma)$ in the intermediate and high mass range, and $f_{1,\beta^{(1)}}^{m-m}(\sigma)$ at low masses. The overall effect of these non-Markovian terms is to reduce the overall amplitude of the Markovian solution.

Notice that the non-Markovian correction $f_{1,\beta=0}^{m-m}(\sigma)$ diverges in the very low mass limit ($\sigma \rightarrow \infty$) due to the behavior of the incomplete Gamma function in Eq. (39). As shown in Fig. 5, this term (short dash line) decreases to a negative minimum value at $\log(1/\sigma) \sim 0$ and then increases in the low mass range, eventually diverging at very small masses, $\log(1/\sigma) \ll -0.6$ (corresponding to $M \ll 10^{10} h^{-1} M_{\odot}$). This implies that the mass function in the case of a diffusive barrier with constant average is ill behaved in the very small mass limit. Hence, in order to extend its validity one should consider the contribution of higher-order corrections in κ . However, as we have previously discussed, the low mass end of the mass function is sensitive to the non-spherical collapse of halos. In such a case the non-Markovian correction due to the average drift of the barrier to leading order in β , $f_{1,\beta^{(1)}}^{m-m}(\sigma)$, cures the divergent behavior of $f_{1,\beta=0}^{m-m}(\sigma)$. This can be inferred directly from Eq. (40), where the dependence on the incomplete Gamma function is of opposite sign to that in Eq. (39). As shown in Fig. 5, $f_{1,\beta^{(1)}}^{m-m}(\sigma)$ (long dash line) decreases towards negative values as $f_{1,\beta=0}^{m-m}(\sigma)$ increases towards positive values for small values of $\log(1/\sigma)$. The dependence on the Gamma function also appears in $f_{1,\beta^{(2)}}^{m-m}(\sigma)$, however this correction is subdominant with respect to $\mathcal{O}(\beta)$. Eventually, one can find a small mass range where higher-order corrections in κ and β cannot be neglected. However, our analysis shows that in the mass range probed by current simulations, $-0.6 < \log(1/\sigma) < 0.4$ (corresponding $10^{10} < M[h^{-1} M_{\odot}] < 10^{15}$) the perturbative expansion in κ and β is well behaved provided $\beta/(1 + D_B) < 1$.

V. EXCURSION SET MASS FUNCTION AND N-BODY SIMULATIONS

The barrier model which we have considered here aims to capture the main features of the ellipsoidal collapse of dark matter halos. It explicitly depends on β and D_B which parametrize the properties of the collapse threshold. In principle, these parameters can be determined for a given ellipsoidal collapse model. This is because the distribution of collapse density values is directly related to the probability distribution of the eigenvalues of the deformation tensor (see e.g. [28, 38]). Alternatively, one can infer such a distribution by numerically solving the ellipsoidal collapse equations for randomly generated initial conditions (see e.g. [39–41]). Then, the values of β and D_B can be inferred by best fitting the average and the variance of the inferred ellipsoidal collapse density distribution.

Most of the works in the literature have primarily focused on determining the average of the ellipsoidal col-

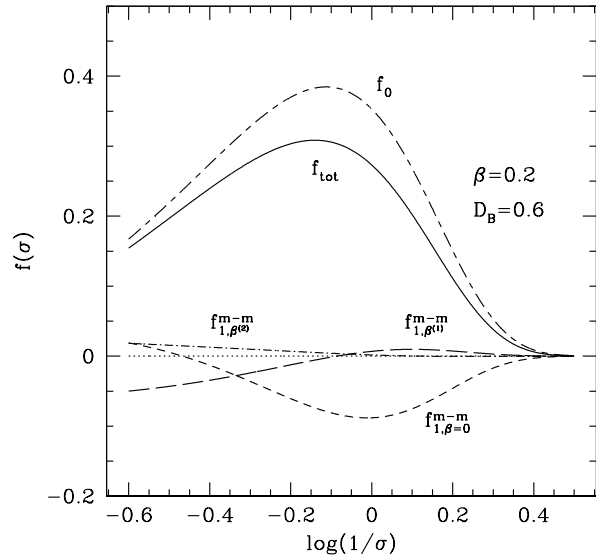


FIG. 5: Contributions to the halo mass function f_{tot} (solid line) for $\beta = 0.2$ and $D_B = 0.6$. The different curves correspond to the Markovian mass function f_0 (dot line) and the non-Markovian corrections $f_{1,\beta=0}^{m-m}$ (short dash line), $f_{1,\beta^{(1)}}^{m-m}$ (long dash line), $f_{1,\beta^{(2)}}^{m-m}$ (dot-short dash line), $f_{1,\beta^{(3)}}^{m-m}$ (dot-long dash line).

lapse threshold [28, 30], while no attention has been paid to the variance. In [21] the authors have provided a rough estimate of the variance from the ellipsoidal collapse barrier numerically determined in [42], though they did not use such estimate when evaluating the mass function. Furthermore, it is very plausible that the distribution collapse densities varies with cosmology and redshift. Hence, an accurate ellipsoidal collapse model prediction of β and D_B requires a dedicated study which is beyond the scope of this paper.

Here, we test whether the path-integral inferred mass function can provide a reasonable description of the numerical simulation data. In order to perform such a test we use the measurements of the halo mass function from Tinker et al. [10] obtained using SOD with $\Delta = 200$ on a set of WMAP-1yr and WMAP-3yr cosmological N-body simulations. First, we consider the mass function measurements at $z = 0$. For the LCDM models best fitting WMAP-1yr and 3yr data the spherical collapse model prediction is $\delta_c = 1.673$. Using such a value we run a likelihood Markov Chain Monte Carlo analysis of the excursion set mass function $f_{\text{tot}}(\sigma)$ including non-Markovian corrections up to $\mathcal{O}(\beta^3)$ against the data to infer the best fit values of β and D_B . The prior parameter space is $\log \beta = [-4, 0]$ and $\log D_B = [-3, 0]$.

We find $\beta = 0.057$ and $D_B = 0.294$ respectively. The numerical simulation data strongly constrain these parameters with 1σ errors $\sigma_\beta = 0.001$ and $\sigma_{D_B} = 0.001$ re-

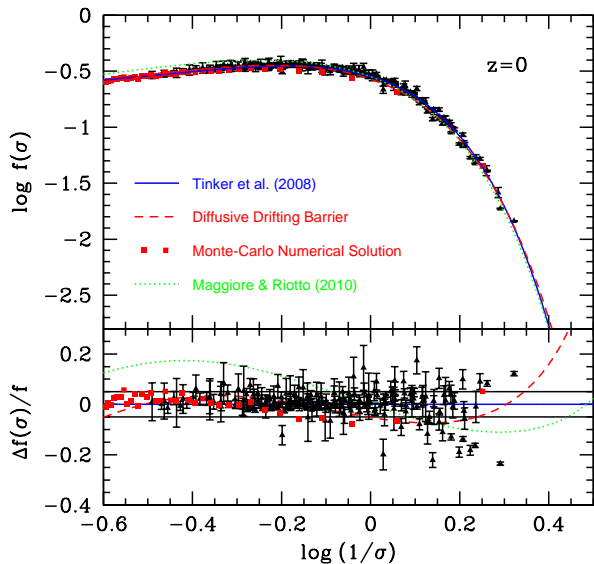


FIG. 6: (Upper panel) Halo mass function at $z = 0$ for the Tinker et al. fitting formula with $\Delta = 200$ (solid blue line), diffusing drifting barrier with $\beta = 0.057$ and $D_b = 0.294$ (red dash line) and the corresponding numerical solution from Monte Carlo generated random walks with sharp-x filter (red squares), Maggiore & Riotto [21] with $D_B = 0.235$ (green dot line). Data points are from [10]. (Lower panel) Relative difference with respect to the Tinker et al. [10] fitting formula. The thin black solid lines indicates 5% deviations.

spectively. We have also verified that these results do not change if corrections $\mathcal{O}(> \beta^3)$ are included in $f_{\text{tot}}(\sigma)$. In Fig. 6 (upper panel) we plot the best fitting mass function (red dash line) against the simulation data together with the four-parameter fitting formula by Tinker et al. [10] for $\Delta = 200$ (solid blue line). For comparison we also plot the diffusive barrier by Maggiore & Riotto [21] best fitting the data with $D_B = 0.235$ (green dot line). In Fig. 6 (lower panel) we plot the relative differences with respect to the Tinker et al. formula. We may notice the remarkable agreement of the diffusive drifting barrier with the data. Deviations with respect to Tinker et al. (2008) are within the $\approx 5\%$ level for $\log(1/\sigma) < 0$ and within 7% over the range $0 < \log(1/\sigma) < 0.3$. This is quite impressive given the fact that our model depends only on two physical parameters. As expected the improvement with respect to the diffusive barrier [21] is due to the drifting average which systematically suppresses the formation of small mass halos with respect to the massive ones. In Fig. 6 we also plot the mass function for the diffusive barrier model with $\beta = 0.057$ and $D_b = 0.294$ inferred from Monte-Carlo generated random walks with sharp-x filtering (red squares). As it can be seen this numerical solution well reproduce our mass function formula with

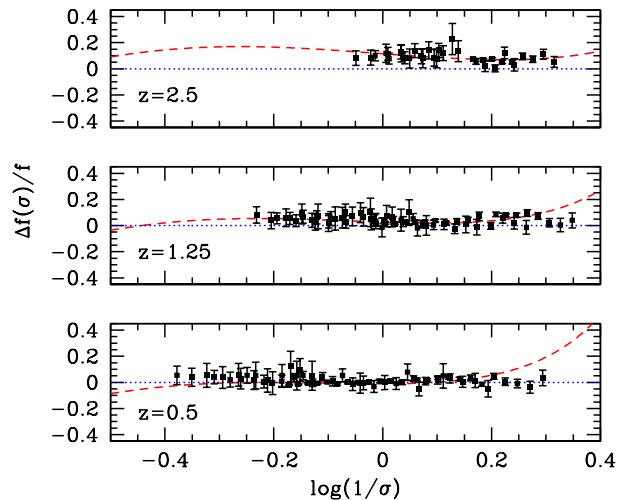


FIG. 7: Redshift evolution of the mass function residuals with respect to the redshift dependent Tinker et al. [10] fitting function (blue solid line) for diffusive barrier with linearly drifting average (red dash line).

the same level of deviations from the Tinker et al. data³.

It is worth noticing that the best fit value of β is about a factor 5 smaller than the ellipsoidal collapse model expectation. This could be an artifact of the SOD mass function measurements, a consequence of our modeling of the barrier diffusion as a Gaussian random walk rather than log-normal, or having limited the non-Markovian corrections to first order in κ . In a future study we will perform a more detailed analysis to discriminate between these different effects. This will allow us to obtain an unbiased physical interpretation of the barrier model parameter values.

The mass function measurements from Tinker et al. [10] extend to $z = 0.5, 1.25$ and 2.5 . The mass function can also reproduce these measurements for a given combination of values of β and D_B . At these redshifts we have $\delta_c = 1.680, 1.685$ and 1.686 respectively [11].

In Fig. 7 we plot the residual of the mass function $f_{\text{tot}}(\sigma)$ for the barrier model parameters best fitting the data at $z = 0.5, 1.25$ and 2.5 with respect to redshift dependent fitting formula by Tinker et al. [10]. We can

³ Recently, in [43] the authors claim that the path-integral approach does not reproduce the Monte-Carlo inferred mass function to no better than 20% and thus conclude that such a formalism is inappropriate to fit halo abundances $dn(M)/dM$. Our numerical evaluation for the diffusive barrier model with linearly drifting average shown in Fig. 6 clearly demonstrates this not to be the case.

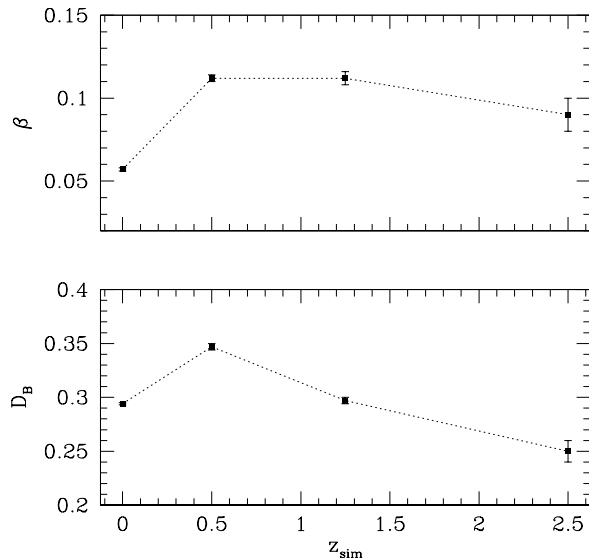


FIG. 8: Best fitting values of β (upper panel) and D_B (lower panel) as function of redshift.

see that, apart a systematic deviation at high masses ($\log(1/\sigma) > 0.2$) of order of $\lesssim 10\%$, $f_{\text{tot}}(\sigma)$ is consistent with data to better than 5%. In particular at $z = 2.5$ the functional form of the halo mass function seems to better reproduce the numerical measurements compared to the Tinker et al. [10] fitting formula for which the authors have found residuals $> 5\%$ at $z = 2.5$. In Fig. 8 we plot the best fit values of β and D_B as function of z . The value of β tends to saturate at $z > 0.5$, which would imply that the non-spherical collapse threshold on average has a similar mass (scale) dependence at higher redshifts than at present. On the other hand, D_B peaks at $z = 0.5$ and then decreases. Since, the diffusion coefficient primarily affect the high-mass end of the mass function, this would suggest that the collapse threshold of massive halos at higher redshifts is closer to that predicted by the spherical collapse. However, because of the limited z -sampling as well as a systematic bias of the mass function data towards high masses the physical interpretation of these trends should be taken carefully. We leave a detailed analysis of these dependencies to a future numerical study.

VI. LINEAR HALO BIAS

Halos are biased tracers of the dark matter density perturbations from which they form. Operationally the halo bias is defined as the ratio of the 2-point halo spatial correlation function to that of the underlying dark matter density fluctuation field. In the Excursion Set formalism this can be estimated using the peak-background

split technique (see e.g. [44–47]) The basic idea is to evaluate the conditional first-crossing distribution and infer the relative abundance of halos of a given mass (i.e. S) as function of the large scale density fluctuation δ_0 , $\mathcal{F}(S|\delta_0, S' = 0)$. Then, it can be shown that to first order in δ_0 the halo bias is given by

$$b_h(S) = 1 + \frac{1}{\mathcal{F}(S|0, 0)} \left. \frac{\partial \mathcal{F}(S|\delta_0, 0)}{\partial \delta_0} \right|_{\delta_0=0}, \quad (42)$$

where $\mathcal{F}(S|0, 0)$ coincides with the unconditional first-crossing distribution with $\delta_0 = 0$.

In the framework of the Excursion Set theory the halo bias for the sharp-x filter with the non-Markovian corrections to first order in κ has been derived in [48]. We extend their calculation to the diffusive barrier with linearly drifting average (see also [49] for the case with sharp-k filter and [50] for a computation of the conditional mass function in the case of generic moving barrier models and sharp-x filter). The calculations are quite cumbersome and since the basic results by Ma et al. [48] applies also to our case, we will report only the relevant passages.

In order to evaluate $\mathcal{F}(S|\delta_0, 0)$ let us first compute the conditional mass function with conditioning on a generic scale $S' < S$ where $\delta(S') \ll B(S')$. We find convenient to work with the variable $Y = B - \delta$, even though the conditional first-crossing distribution $\mathcal{F}(S|\delta', S')$ differs from $\mathcal{F}(S|Y', S')$. In fact, the latter imposes the condition on both variables δ and B , while the former does not impose any condition on the barrier value. Nevertheless, since we are interested in computing the first-crossing distribution in the large scale limit, the barrier trajectories converge toward a unique constant value, $B_0 = \delta_c$ for $S' \rightarrow 0$ and thus we recover $\mathcal{F}(S|\delta_0, 0)$. Nevertheless, some care is needed when computing the non-Markovian corrections.

Following [48] the path-integral definition of the conditional first-crossing distribution is

$$\mathcal{F}(S_n|Y_m, S_m) = - \int_0^\infty dY_n \frac{\partial P(Y_n, S_n|Y_m, S_m)}{\partial S_n}, \quad (43)$$

where

$$\begin{aligned} P(Y_n, S_n|Y_m, S_m) &\equiv \\ &\equiv \frac{\int_0^\infty dY_1 \dots d\hat{Y}_m \dots dY_{n-1} W(Y_0 = \delta_c, \dots, \hat{Y}_m = 0, \dots, Y_n, S_n)}{\int_0^\infty dY_1 \dots dY_{m-1} W(Y_0 = \delta_c, \dots, Y_m, S_m)} \end{aligned} \quad (44)$$

with the probability density developed to first order in κ reads as

$$W(\dots) = W_0(\dots) + \frac{1}{2} \sum_{i,j=1}^n \Delta_{ij} \partial_i \partial_j W_0(\dots), \quad (45)$$

and $W_0(\dots)$ is the probability density distribution of the discrete Markovian random walks. Notice that the integral in the denominator of Eq. (44) provides the correct

normalization factor to the conditional first-crossing distribution. The numerator in Eq. (44) can be computed by splitting the sum in Eq. (45) and computing each term individually. However, as shown in [48] only few of these terms actually contribute to $\mathcal{F}(S_n|Y_m, S_m)$ and we have verified this to be the case also for the diffusive barrier model with linearly drifting average. In particular we have

$$P(Y_n, S_n|Y_m, S_m) = \Pi_0(Y_m, Y_n, S_n - S_m) + \Pi_1^a(Y_m, Y_n, S_n - S_m) + \frac{N_1^b(Y_m, Y_n, S_m, S_n)}{\Pi_0(Y_0 = \delta_c, Y_m, S_m)} \quad (46)$$

where $\Pi_0(Y_m, Y_n, S_n - S_m)$ and $\Pi_0(Y_0 = \delta_c, Y_m, S_m)$ are given by the Markovian probability distribution Eq. (16). The other two terms in Eq. (46) contains the non-Markovian corrections to first order in κ , these read as

$$\begin{aligned} \Pi_1^a(Y_m, Y_n, S_n - S_m) &= \frac{1}{2} \sum_{i,j=m+1}^{n-1} \Delta_{ij} \int_0^\infty dY_{m+1} \dots \int_0^\infty dY_{n-1} \partial_i \partial_j W_0(Y_m, \dots, Y_n, S_n - S_m) = \\ &= \sum_{i,j=m+1}^{n-1} \Delta_{ij} \Pi_0^\epsilon(Y_m, 0, S_i - S_m) \Pi_0^\epsilon(0, 0, S_j - S_i) \Pi_0^\epsilon(0, Y_n, S_n - S_j), \end{aligned} \quad (47)$$

and

$$\begin{aligned} N_1^b(Y_m, Y_n, S_n, S_m) &= \sum_{j=m+1}^{n-1} \Delta_{jm} \int_0^\infty dY_1 \dots dY_j \dots \int_0^\infty dY_{n-1} \partial_m W_0(\delta_c, \dots, Y_m, S_m) W_0(Y_m, \dots, Y_j, S_j - S_m) \times \\ &\times W_0(Y_j, \dots, Y_n, S_n - S_j) = \partial_m \Pi_0(Y_0 = \delta_c, Y_m, S_m) \sum_{j=m+1}^{n-1} \Delta_{jm} \Pi_0^\epsilon(Y_m, 0, S_j - S_m) \Pi_0^\epsilon(0, Y_n, S_n - S_j). \end{aligned} \quad (48)$$

As in the case of the non-Markovian corrections to the mass function, these terms can be computed in the continuous limit with the sum substituted with an integral over the variance and the integrands given by Eq. (29), (31) and (32) respectively.

The first term in Eq. (46) gives the Markovian conditional first-crossing distribution. In the limit $S_m \rightarrow 0$ (i.e. $Y_m \rightarrow \delta_c - \delta_0$) we find

$$\mathcal{F}_0(S|\delta_0, 0) = \frac{(\delta_c - \delta_0)}{S^{3/2}} \sqrt{\frac{a}{2\pi}} e^{-a \frac{(\delta_c - \delta_0 + \beta S)^2}{2S}} \quad (49)$$

Eq. (47) is equivalent to the ‘memory-of-memory’ term Eq. (37) In the limit $S_m \rightarrow 0$. The double integral over the variance can be computed analytically by Taylor expanding in β . Here, we limit the computations to terms up to first order in β , since its numerically calibrated value is $\approx 10^{-2}$. We find

$$\begin{aligned} \mathcal{F}_{1,\beta=0}^a(S|\delta_0, 0) &= -\tilde{\kappa} \frac{(\delta_c - \delta_0)}{S^{3/2}} \sqrt{\frac{a}{2\pi}} \times \\ &\times \left[e^{-a \frac{(\delta_c - \delta_0)^2}{2S}} - \frac{1}{2} \Gamma \left(0, \frac{a(\delta_c - \delta_0)^2}{2S} \right) \right] \end{aligned} \quad (50)$$

and

$$\begin{aligned} \mathcal{F}_{1,\beta(1)}^a(S|\delta_0, 0) &= -\beta a (\delta_c - \delta_0) \left[\mathcal{F}_{1,\beta=0}^a(S|\delta_0, 0) + \right. \\ &\left. + \frac{\tilde{\kappa}}{2S} \text{Erfc} \left(\frac{\delta_c - \delta_0}{\sqrt{2S}} \sqrt{a} \right) \right] \end{aligned} \quad (51)$$

On the other hand, the computation of Eq. (48) requires some care. This term contains the derivative of the Markovian solution, $\Pi_0(\delta_c, Y_m, S_m)$, with respect to Y_m , hence it explicitly depends on the variation of the probability distribution with respect to the distance of the barrier B_m to δ_m . Nonetheless, we are interested in the first-crossing distribution which is conditional in δ_m only, and for which the result of the integration of Eq. (48) in the limit $S_m \rightarrow 0$ should depend only on the variation with respect to δ_m . However, after computing this term we find that for $\beta = D_B = 0$ we do not recover the non-Markovian correction of spherical collapse model. This is a direct consequence of the fact that we are working with Y rather than δ . The correct way to proceed is to first marginalize over B_m and then take the limit $S_m \rightarrow 0$. However, this is a very cumbersome computation, instead we have found that the inconsistency can be cured by simply taking the derivative in Eq. (48)

with respect to δ_m only. In such a case we find

$$\mathcal{F}_{1,\beta=0}^b(S|\delta_0, 0) = -\tilde{\kappa} \frac{\delta_0}{S^{3/2}} \sqrt{\frac{a}{2\pi}} \times e^{-a \frac{(\delta_c - \delta_0)^2}{2S}} \left\{ 1 - a \frac{(\delta_c - \delta_0)^2}{S} \right\}, \quad (52)$$

which for $D_B = 0$ coincides with the result of [48] and

$$\mathcal{F}_{1,\beta(1)}^b(S|\delta_0, 0) = -\beta a \tilde{\kappa} \frac{\delta_0(\delta_c - \delta_0)}{S^{3/2}} 2 \sqrt{\frac{a}{2\pi}} \times e^{-a \frac{(\delta_c - \delta_0)^2}{2S}} \left\{ 1 - a \frac{(\delta_c - \delta_0)^2}{S} \right\}, \quad (53)$$

Then, summing all these terms and evaluating Eq. (42) we finally obtain

$$b_h(\nu) = 1 + \frac{1}{\delta_c} \frac{a\nu^2 - 1 + \frac{\tilde{\kappa}}{2} \left[2 - e^{\frac{a\nu^2}{2}} \Gamma\left(0, \frac{a\nu^2}{2}\right) \right]}{1 - \tilde{\kappa} + \frac{\tilde{\kappa}}{2} e^{\frac{a\nu^2}{2}} \Gamma\left(0, \frac{a\nu^2}{2}\right)} + \frac{\beta a}{\left[1 - \tilde{\kappa} + \frac{\tilde{\kappa}}{2} e^{\frac{a\nu^2}{2}} \Gamma\left(0, \frac{a\nu^2}{2}\right) \right]^2} \times \left\{ 1 - \tilde{\kappa} \left[a\nu^2 + 2 - e^{\frac{a\nu^2}{2}} \Gamma\left(0, \frac{a\nu^2}{2}\right) - e^{\frac{a\nu^2}{2}} \sqrt{\frac{a\pi}{2}} \text{Erfc}\left(\frac{\nu\sqrt{a}}{2}\right) \right] \right\}, \quad (54)$$

where $\nu = \delta_c/\sigma$. In Fig. 9 we plot the halo bias for β and D_B best fitting the mass function data at $z = 0$ (red short dash line) against the best fit formula to the bias measurements inferred in [51] (black solid line). As we can see the difference is $\lesssim 20\%$ over the mass range probed by the simulations. This is consistent with the findings of Ma et al. [48]. As argued in [51] the discrepancy with respect to the halo bias data from N-body simulations is related to the peak-background split approximation itself. Hence, the improvement on mass function calculation does not give any further insight on the linear halo bias.

VII. CONCLUSIONS

The Excursion Set formalism provides a powerful mathematical framework which allows us to perform a theoretical computation of the halo mass function from a limited set of initial assumptions. These must involve the statistics of the linear density fluctuation field as well as a stochastic barrier model of the halo collapse conditions. In addition, such calculation needs to be implemented with a path-integral evaluation of the corrections due to the filtering of the linear density field associated with a realistic mass definition. Such an approach allows for a consistent model comparison with N-body simulation data.

Here, we have derived an analytical expression for the mass function and linear bias in the case of a diffusive

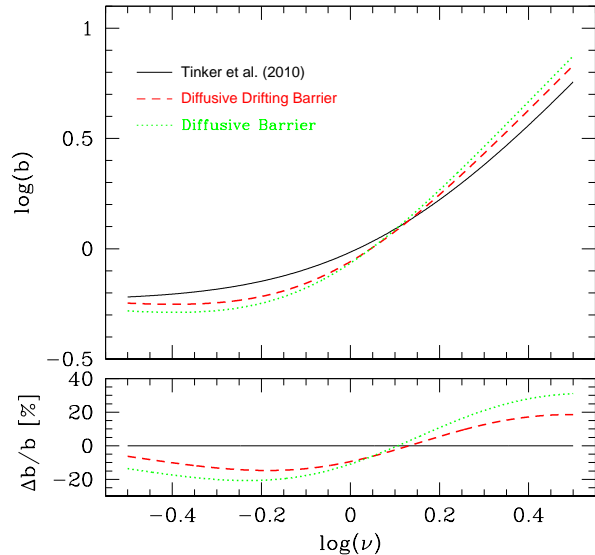


FIG. 9: Top panel: Halo bias for the diffusive drifting barrier model with parameters best fitting mass function data from [10] at $z = 0$ (red short dash line) against the best fit formula to the halo bias from the same numerical simulation sets inferred in [51] (black solid line). Lower panel: relative difference with respect to the halo fit formula from [51].

barrier model with linearly drifting average. This model well approximates the main features of the ellipsoidal collapse. We have found a remarkable agreement with N-body simulation data with differences $\approx 5\%$ over a large range of masses. Such an agreement is due to the competing effects of the barrier average drift at small masses and of the diffusion in the high-mass end. This has important phenomenological implications especially in the study of primordial non-Gaussianity. In fact, several studies have estimated the halo mass function in the case of non-Gaussian initial conditions assuming the spherical collapse models (see e.g. [5, 6, 52]). However the comparison with non-Gaussian N-body simulations has shown large deviations in the low mass range compared to large masses (see e.g. Fig. 1 in [53]). In the light of our results, it is plausible that such discrepancies may be attributed to the non-spherical collapse of halos. The inclusion of a simple diffusive barrier model with linearly drifting average for a non-Gaussian linear density field could resolve or alleviate the problem.

Our results suggest a number of directions which warrant further investigation. Firstly, it will be insightful to derive the statistical properties of the fuzzy barrier for a given ellipsoidal model as function of the variance of the linear density field. This will provide theoretical predictions for β and D_B which can be confronted with numerically calibrated values for different redshifts and cosmologies, and it will allow us to accurately testing the modeling of the halo collapse conditions. On the

other hand, in the upcoming years several observational campaigns will probe the halo abundance through galaxy cluster surveys. The mass function derived here can be used to perform a data analysis of the barrier model parameters, thus providing information on the collapse of DM halos which has been previously unforeseen.

Acknowledgments

We are especially thankful to J. Tinker for kindly providing us with the mass function data. It is a pleasure to thank J.-M. Alimi, L. Amendola, M. Maggiore, Y. Rasera, T. Riotto and R. Sheth for useful discussions. I. Achitouv is supported by a scholarship of the ‘Ministère de l’Education Nationale, de la Recherche et de la Technologie’ (MENRT).

Appendix A: Chapman-Kolmogorov Equation

The probability density distribution of the discrete Markovian random walk is given by Eq. (24) which by expliciting the variance dependence of the connected 1 and 2-point correlators reads as

$$W_0(Y_0, \dots, Y_n, S_n) = \int \mathcal{D}\lambda e^{i \sum_i \lambda_i (Y_i - \bar{B}_i) - \frac{\epsilon}{2} \sum_{ij} \lambda_i \lambda_j \tilde{A}_{ij}}, \quad (\text{A1})$$

where $\tilde{A}_{ij} = (1 + D_B) \min(i, j)$. Diagonalizing the quadratic form in Eq. (A1) and solving the resulting Gaussian integral we obtain

$$W_0(Y_0, \dots, Y_n, S_n) = \frac{e^{-\frac{1}{2\epsilon(1+D_B)} \sum_{ij} (Y_i - \bar{B}_i) A_{ij}^{-1} (Y_j - \bar{B}_j)}}{[2\pi\epsilon(1 + D_B)]^{\frac{n}{2}}}, \quad (\text{A2})$$

where $A_{ij} = \min(i, j)$. One can show through induction that $(A^{-1})_{ij} = 2$ for $i = 1, \dots, n-1$, $(A^{-1})_{nn} = 1$ and $(A^{-1})_{i, i+1} = (A^{-1})_{i+1, i} = -1$ for $i = 1, \dots, n-1$, while all other elements vanish. Similarly one finds that $\det A = 1$. Thus, we can write Eq. (A2) as

$$W_0(Y_0, \dots, Y_n, S_n) = \frac{e^{-\frac{1}{2\epsilon(1+D_B)} \sum_{i=1}^{n-1} [(Y_{i+1} - Y_i) - (\bar{B}_{i+1} - \bar{B}_i)]^2}}{[2\pi\epsilon(1 + D_B)]^{\frac{n}{2}}} \\ = \psi_\epsilon(\Delta Y) W_0(Y_0, \dots, Y_{n-1}, S_{n-1}), \quad (\text{A3})$$

with $\Delta Y = Y_n - Y_{n-1}$ and

$$\psi_\epsilon(\Delta Y) = \frac{1}{\sqrt{2\pi\epsilon(1 + D_B)}} e^{-\frac{(\Delta Y - \beta\epsilon)^2}{2\epsilon(1+D_B)}}. \quad (\text{A4})$$

An important consequence of the above relations is that the Markovian probability density satisfies the relation:

$$W_0(Y_0, \dots, \hat{Y}_i = 0, \dots, Y_n, S_n) = W_0(Y_0, \dots, Y_{i-1}, 0, S_i) \times \\ \times W_0(0, Y_{i+1}, \dots, Y_n, S_n - S_i) \quad (\text{A5})$$

Finally, from Eq. (21) we obtain the relation

$$\Pi_0^\epsilon(Y_0, Y_n, S_n) = \int_0^\infty dY_{n-1} \psi_\epsilon(\Delta Y) \Pi_0^\epsilon(Y_0, Y_{n-1}, S_{n-1}), \quad (\text{A6})$$

which is the Chapman-Kolmogorov equation for a Gaussian random walk with linearly drifting average.

Appendix B: Calculation of γ

We can compute the factor γ defined by Eq. (30) simply using the properties of the Markovian solution to the Fokker-Planck equation Eq. (15). Without loss of generality we can consider the case where the absorbing boundary is at $Y = Y_c < 0$ rather than $Y = 0$. In such a case the solution to Eq. (15) with initial condition at $Y = Y_0 > Y_c$ reads as

$$\tilde{\Pi} = \frac{e^{a\beta(Y - Y_0 - \beta\frac{S}{2})} \sqrt{a}}{\sqrt{2\pi S}} \left[e^{-\frac{a(Y - Y_0)^2}{2S}} - e^{-\frac{a(2Y_c - Y - Y_0)^2}{2S}} \right], \quad (\text{B1})$$

where $a = 1/(1 + D_B)$. Taking the derivative with respect to Y_c we have

$$\frac{\partial \tilde{\Pi}}{\partial Y_c} = a \sqrt{\frac{2a}{\pi}} \frac{2Y_c - Y_0 - Y}{S^{3/2}} e^{a\beta(Y - Y_0 - \beta\frac{S}{2})} e^{-\frac{a(2Y_c - Y_0 - Y)^2}{2S}}. \quad (\text{B2})$$

On the other hand using the path-integral formulation we have

$$\tilde{\Pi}_\epsilon = \int_{Y_c}^\infty dY_1 \dots \int_{Y_c}^\infty dY_{n-1} W(Y_0, \dots, Y_n, S_n), \quad (\text{B3})$$

thus

$$\frac{\partial \tilde{\Pi}_\epsilon}{\partial Y_c} = - \sum_i \int_{Y_c}^\infty dY_1 \dots \int_{Y_c}^\infty dY_{n-1} W(Y_0, \dots, \hat{Y}_i, \dots, Y_n, S_n), \quad (\text{B4})$$

then using Eq. (A5) and taking the continuous limit we obtain

$$\frac{\partial \tilde{\Pi}}{\partial Y_c} = - \lim_{\epsilon \rightarrow 0} \frac{1}{\epsilon} \int_0^S dS_i \Pi_\epsilon(0, Y_c, S_i) \Pi_\epsilon(Y_c, Y, S - S_i), \quad (\text{B5})$$

where the left-hand side is given by Eq. (B2), while $\tilde{\Pi}_\epsilon(0, Y_c, S_i)$ and $\tilde{\Pi}_\epsilon(Y_c, Y, S - S_i)$ are the finite- ϵ corrections to the Markovian solution near the boundary. As shown in Section IV B these terms can be evaluated by introducing the stretch variable $\eta\sqrt{2\epsilon/a}$ and expanding the Markovian solution to lowest order in ϵ , this gives

$$\tilde{\Pi}_\epsilon(Y_0, Y_c, S) = \sqrt{\epsilon} \frac{\gamma a (Y_c - Y_0)}{S^{3/2}} e^{-\frac{a(Y_0 - Y_c + \beta S)^2}{2S}}, \quad (\text{B6})$$

and

$$\tilde{\Pi}_\epsilon(Y_c, Y, S) = \sqrt{\epsilon} \frac{\gamma a (Y_c - Y)}{S^{3/2}} e^{-\frac{a(Y - Y_c - \beta S)^2}{2S}}. \quad (\text{B7})$$

Substituting these solutions on the right-hand-side of Eq. (B5) we have

$$\begin{aligned} \frac{\partial \tilde{\Pi}}{\partial Y_c} &= -(a\gamma)^2 (Y_c - Y_0)(Y_c - Y) e^{a\beta(Y - Y_0 - \beta \frac{S}{2})} \times \\ &\times \int_0^{S_n} dS_i \frac{e^{-\frac{a(Y - Y_c)^2}{2(S - S_i)}} e^{-\frac{a(Y_0 - Y_c)^2}{2S_i}}}{S_i^{3/2} (S - S_i)^{3/2}}, \end{aligned} \quad (\text{B8})$$

the integral in dS_i can be computed analytically since

$$\int_0^S dS_i \frac{e^{-\frac{A^2}{2S_i} - \frac{B^2}{2(S - S_i)}}}{S_i^{3/2} (S - S_i)^{3/2}} = \sqrt{2\pi} \frac{A + B}{AB} \frac{1}{S^{3/2}} e^{-\frac{(A+B)^2}{2S}}, \quad (\text{B9})$$

then, substituting in Eq. (B8) and comparing with Eq. (B2) after simplifications we obtain $\gamma = 1/\sqrt{\pi}$.

Appendix C: Non-Markovian Corrections

Using Eq. (34) the non-Markovian correction to first order in κ , Eq. (33), has two separate contributions

$$\begin{aligned} \Pi_{\epsilon,1}^{\text{m}}(Y_0, Y_n, S_n) &= \sum_i \Delta_{in} \partial_n \left[\int_0^\infty dY_1 \dots \int_0^\infty dY_{n-1} \partial_i W_0(Y_0, \dots, Y_n, S_n) \right] \\ &= - \sum_i \Delta_{in} \partial_n \left[\int_0^\infty dY_1 \dots d\hat{Y}_i \dots \int_0^\infty dY_{n-1} W_0(Y_0, \dots, \hat{Y}_i = 0, S_i) W_0(\hat{Y}_i = 0, \dots, Y_n, S_n - S_i) \right] \\ &= - \sum_i \Delta_{in} \partial_n \left[\Pi_0^\epsilon(Y_0, 0, S_i) \Pi_0^\epsilon(0, Y_n, S_n - S_i) \right]. \end{aligned} \quad (\text{C1})$$

where we have used Eq. (A5), and

$$\begin{aligned} \Pi_{\epsilon,1}^{\text{m-m}}(Y_0, Y_n, S_n) &= \sum_{i < j} \Delta_{ij} \int_0^\infty dY_1 \dots \int_0^\infty dY_{n-1} \partial_i \partial_j \left[W_0(Y_0, \dots, Y_n, S_n) \right] \\ &= - \sum_i \Delta_{in} \int_0^\infty dY_1 \dots d\hat{Y}_j \dots \int_0^\infty dY_{n-1} \partial_i \left[W_0(Y_0, \dots, \hat{Y}_j = 0, \dots, Y_n, S_n) \right] \\ &= \sum_{i < j} \Delta_{ij} \int_0^\infty dY_1 \dots d\hat{Y}_i \dots d\hat{Y}_j \dots \int_0^\infty dY_{n-1} \left[W_0(Y_0, \dots, \hat{Y}_i = 0, \dots, \hat{Y}_j = 0, S_j) W_0(\hat{Y}_i = 0, \dots, Y_n, S_n - S_j) \right] \\ &= \sum_{i < j} \Delta_{ij} \left[\Pi_0^\epsilon(Y_0, 0, S_i) \Pi_0^\epsilon(0, 0, S_j - S_i) \Pi_0^\epsilon(0, Y_n, S_n - S_j) \right]. \end{aligned} \quad (\text{C2})$$

[1] D. N. Spergel *et al.*, *Astrophys. J. Suppl.* **148**, 175 (2003).
[2] M. Tegmark *et al.*, *Phys. Rev. D.* **69**, 103501 (2004).
[3] D. Clowe *et al.*, *Astrophys. J.* **648**, L109 (2006).
[4] R. Massey *et al.*, *Nature* **445**, 286 (2007).
[5] M. Lo Verde, A. Miller, S. Shandera & L. Verde, *JCAP* **04**, 014 (2008).
[6] M. Maggiore & T. Riotto, *Astrophys. J.* **717**, 526 (2010).
[7] G. D'Amico, M. Musso, J. Norena & A. Paranjape, *JCAP* **02**, 001 (2011).

[8] M. Pierre *et al.*, *Mont. Not. Roy. Astron. Soc.* in press, arXiv:1009.3182.
[9] F.W. High *et al.* (2010), arXiv:1003.005; T.A. Marriage *et al.*, (2010), arXiv:1010.1065.
[10] J. L. Tinker *et al.*, *Astrophys. J.* **688**, 709 (2008).
[11] J. Courtin *et al.*, *Mont. Not. Roy. Astron. Soc.* in press, arXiv:1001.3425.
[12] M. Crocce *et al.*, *Mont. Not. Roy. Astron. Soc.* **403**, 1353 (2010).

- [13] B. Suman *et al.*, *Astrophys. J.* in press, arXiv:1005.2239.
- [14] W. H. Press & P. Schechter, *Astrophys. J.* **187**, 425 (1974).
- [15] J. E. Gunn & J. R. Gott, III, *Astrophys. J.* **176**, 1 (1972).
- [16] J. A. Peacock & A. F. Heavens, *Mont. Not. Roy. Astron. Soc.* **243**, 133 (1990).
- [17] J. R. Bond, S. Cole, G. Efstathiou & G. Kaiser, *Astrophys. J.* **379**, 440 (1991).
- [18] A. R. Zentner, *Int. J. Mod. Phys. D* **16**, 763 (2007).
- [19] W.J. Percival, *Mont. Not. R. Astron. Soc.* **327**, 1313 (2001).
- [20] M. Maggiori & A. Riotto, *Astrophys. J.* **711**, 907 (2010).
- [21] M. Maggiori & A. Riotto, *Astrophys. J.* **717**, 515 (2010).
- [22] P. S. Corasaniti & I. Achitouv, arXiv:arXiv:1012.3468.
- [23] A. G. Doroshkevich, *Astrophysika* **3**, 175 (1970).
- [24] D. J. Eisenstein & A. Loeb, *Astrophys. J.* **439**, 520 (1995).
- [25] P. Monaco, *Astrophys. J.* **447**, 23 (1995).
- [26] E. Audit, R. Teyssier & J.-M. Alimi, *Astron. & Astrophys.* **325**, 439 (1997).
- [27] J. Lee & S. Shandarin, *Astrophys. J.* **500**, 14 (1998).
- [28] R. K. Sheth, H. J. Mo & G. Tormen, *Mont. Not. Roy. Astron. Soc.* **323**, 1 (2001).
- [29] R. K. Sheth, *Mont. Not. Roy. Astron. Soc.* **300**, 1057 (1998).
- [30] J. Shen, T. Abel, H. J. Mo & R. K. Sheth, *Astrophys. J.* **645**, 783 (2006).
- [31] S. Furlanetto & S. Oh, *Mont. Not. Roy. Astron. Soc.* **363**, 1031 (2005).
- [32] J. Zhang & L. Hui, *Astrophys. J.* **641**, 641 (2006).
- [33] B. Robertson, A. Kravtsov, J. Tinker & A. Zentner, *Astrophys. J.* **696**, 636 (2009).
- [34] N. G. Van Kemp, “Stochastic Processes in Physics and Chemistry”, North-Holland Personal Library (1992).
- [35] S. Redner, “A guide to first-passage processes”, Cambridge University Press, (2001).
- [36] U. Seljak and M. Zaldarriaga, *Astrophys. J.* **469**, 437 (1996).
- [37] N. Sugiyama, *Astrophys. J. Supp.* **100**, 281 (1995).
- [38] J. R. Bond & S. T. Myers, *Astrophys. J. Supp.* **103**, 1 (1996).
- [39] T. Chiueh & J. Lee, *Astrophys. J.* **555**, 83 (2001).
- [40] R. K. Sheth & G. Tormen, *Mont. Not. Roy. Astron. Soc.* **329**, 61 (2002).
- [41] V. Desjacques, *Mont. Not. Roy. Astron. Soc.* **388**, 638 (2008).
- [42] H. B. Sandvik, O. Moller, J. Lee & S. D. White, *Mont. Not. Roy. Astron. Soc.* **377**, 234 (2007)
- [43] A. Paranjape, T. Y. Lam & R.K. Sheth, arXiv:1105.1990
- [44] J. M. Bardeen, J. R. Bond, N. Kaiser & A. Szalay, *Astrophys. J.* **304**, 15 (1986).
- [45] S. Cole & N. Kaiser, *Mont. Not. Roy. Astron. Soc.* **237**, 1127 (1989).
- [46] H. Mo & S. White, *Mont. Not. Astron. Soc.* **282**, 347 (1996).
- [47] R. K. Sheth & G. Tormen, *Mont. Not. Roy. Astron. Soc.* **308**, 119 (1999).
- [48] C.-P. Ma, M. Maggiori, A. Riotto & J. Zhang, *Mont. Not. Roy. Astron. Soc.* **411**, 2644 (2011).
- [49] J. Zhang, C.-P. Ma, O. Fakhouri, *Mont. Not. Roy. Astron. Soc.* **387**, L13 (2008).
- [50] A. de Simone, M. Maggiori & A. Riotto, *Mont. Not. Roy. Astron. Soc.* in press, arXiv:1007.1903.
- [51] J. L. Tinker et al., *Astrophys. J.* **724**, 878 (2010).
- [52] S. Matarrese, L. Verde & R. Jimenez, *Astrophys. J.* **541**, 10 (2000).
- [53] T. Giannantonio & C. Porciani, *Phys. Rev. D* **81**, 063530 (2010).